Journal of Nuclear Materials 448 (2014) 487–496

Contents lists available at ScienceDirect

Journal of Nuclear Materials

journal homepage: www.elsevier.com/locate/jnucmat

Irradiation creep of 3C–SiC and microstructural understanding of the underlying mechanisms

Sosuke Kondo *, Takaaki Koyanagi, Tatsuya Hinoki

Institute of Advanced Energy, Kyoto University, Japan

ARTICLE INFO

Article history:
Available online 11 September 2013

ABSTRACT

Irradiation-induced creep in high-purity silicon carbide was studied by an ion-irradiation method under various irradiation conditions. The tensioned surfaces of bent thin specimens were irradiated with 5.1 MeV Si^{2+} ions up to 3 dpa at 280–1200 °C, which is referred to as a single-ion experiment. Additional He^{+} ions were irradiated simultaneously in the dual-ion experiment to study the effects of transmuted helium on irradiation creep. Irradiation creep was observed above 400 °C in the single-ion case, where a linear relationship between irradiation creep and swelling (C/S) was observed at 400–800 °C for all stress levels (150, 225, and 300 MPa). The proportional constant of the C/S relationship was strongly dependent on temperature and stress. A rapid reduction in creep strain was observed above 1000 °C. On the basis of the microstructural analysis, anisotropic distribution of self-interstitial atom (SIA) clusters was suspected to be the primary creep mechanism. Some interesting results were obtained from re-irradiation under stress after the irradiation without stress. The creep strain was significantly retarded by pre-irradiation to even 0.01 dpa at 400 and 600 °C. This implies that the loop orientation was determined very early in the irradiation regime. For the dual-ion cases, irradiation creep was absent or very limited at all irradiation temperatures studied (400–800 °C). Microstructural analysis indicated that helium inhibited the stable growth of SIA clusters and prevented them from exhibiting anisotropic distribution.

1. Introduction

The outstanding chemical stability and strength of silicon carbide (SiC) at high temperatures have stimulated the research activity that aims to use SiC, especially 3C-SiC, for functional materials in nuclear applications. So far, excellent irradiation stability has been reported for SiC at wide temperature ranges and damage levels under neutron irradiation. Most irradiation properties of 3C–SiC such as swelling, microstructural development, thermal property, and irradiated strength have been summarized in [1] and more recently in [2]. Because microstructural development, including swelling, is one of the most basic properties and historically the key irradiation property, it has been extensively studied by various irradiation methods such as neutron- [3], electron- [4], and ion-irradiation experiments [5]. Swelling itself is not considered to limit the operating temperature of the nuclear reactors either at the upper or lower temperature limit. However, a significant internal shear stress may be introduced in the irradiated structure, such as the flow-channel-insert wall for nuclear fusion applications, through differential swelling induced by the through-thickness temperature gradient [6]. Irradiation creep, more accurately irradiation-induced creep in SiC, may be indispensable to mitigate internal stress because of the extremely limited rates of thermal creep below ~1000 °C. Furthermore, irradiation creep is one of the key mechanical properties to use in a reactor core such as a TRISO (tri-structural isotropic) coated fuel particle for gas cooled reactors and fuel cladding for light water reactors. Despite this, irradiation creep data is somewhat scarce for SiC primarily because of the difficulty of the stress loading under neutron irradiation.

So far, many irradiation techniques have been developed to evaluate irradiation creep of SiC, and the methods and results are briefly reviewed here. In the first irradiation creep experiment for SiC by Price, pyrolytic 3C-SiC, coated on oriented graphite substrates, was irradiated with neutrons at 640 and 900 °C [7]. The results using dynamic stress loading were perhaps complex, but the upper limit of the steady creep constant was inferred. In the subsequent experiment by Price, thin SiC strips were irradiated with neutrons in four-point flexural loading fixtures at 780, 950, and 1130 °C [1]. By measuring the residual curvature of the irradiated specimens after releasing them from the fixtures, the linear relationship between stress and strain was demonstrated. According to the work by Scholts [8], SiC fibers, consisting of a 33-μm-diameter carbon core covered by SiC layers totaling 50 μm in thickness, were irradiated with 14 MeV deuterons at 450, 600, and 800 °C under torsion stress, where controlled torque was applied to a specimen using a coil inside a permanent magnet. In that work, the temperature dependence of torsion creep rates was re-

* Corresponding author. Tel.: +81 776 38 4560; fax: +81 776 38 4561.
E-mail address: kondo@iae.kyoto-u.ac.jp (S. Kondo).

0022-3115/$ - see front matter
http://dx.doi.org/10.1016/j.jnucmat.2013.09.004

ported to be similar to that of swelling. Katoh and Snead recently evaluated the irradiation creep of high-purity SiC using the bend stress relaxation (BSR) method [9], where creep strain was estimated on the basis of the residual curvature of the irradiated specimen after irradiation. They pointed out the significant importance of understanding irradiation creep at an early stage of irradiation because strain rates are significant.

The data previously reported are, of course, valuable and can provide key insights to irradiation creep of SiC, but directly comparing these data seemed somewhat inadequate because of differences in both the stress loading methods and materials (i.e., purity and fabrication process). Variations in the species and conditions of the irradiated particles can also significantly affect the results. Therefore, systematical irradiation experiments under well-controlled irradiation conditions using samples of identical quality may be essential to understand trends of irradiation creep. The ion-irradiation method reliably meets the highly controllable requirements of the irradiation conditions, with additional advantages of saving time and cost. The irradiation creep of high-purity SiC is studied using the methods developed in the present work to obtain a basic understanding of dependence of key irradiation conditions on the irradiation creep. In addition, the underlying mechanisms are discussed on the basis of the microstructural analysis results.

2. Experimental technique

Bend stress was applied to the irradiated surface of thin SiC specimens by a technique similar to the BSR technique for neutron irradiation experiments [9]. However, the experimental and evaluation techniques of this work are somewhat different in design compared with the BSR technique, primarily due to a very limited ion range for this work (~3.5 μm from the irradiated surface). In the present work, irradiation-induced deformation at the surface bent the whole specimen, including the unirradiated substrate, after it was released from the fixtures. Because the irradiated curvature contains information on strain mismatch between the irradiated and unirradiated regions, the irradiation-induced strain can logically be estimated from the curvature if the relationship between strain and curvature is adequately analyzed. In this section, the relationship between strain and curvature is discussed for specimens irradiated without applied stress, following general descriptions of the materials, fixtures, and irradiation conditions.

2.1. Specimens and fixtures

The material used was polycrystalline 3C–SiC produced by chemical vapor deposition by Rohm and Haas (current subsidiary of Dow Chemical Co., Marlborough, Massachusetts). The chemical vapor deposited (CVD) SiC was of very high purity, with typical total metal impurity concentration less than 5 wppm. The typical grain size was between 5 and 10 μm in the plane parallel to the deposition substrate, with grains elongated in the ⟨1 1 1⟩ growth direction perpendicular to the substrate. The material was essentially free of micropores, microcracks, or other large flaws, but atomic layer stacking faults on the {1 1 1} planes were common. The density measured using Archimedes' principle was in good agreement with the theoretical density (3.21 g/cm^3).

Specimens and fixtures are shown in Fig. 1. The specimens, with dimensions of 1.5 mm width and 3.0 mm length, were mechanically thinned and lap finished on both surfaces, aiming to obtain 50, 75, and 100 μm thicknesses. The machining errors on the thickness were less than ±1 μm. Each specimen was sandwiched between upper and lower fixtures in the order shown schematically in Fig. 1 (b). A curvature of radius 75 mm was provided on an inner surface, which contacted the specimen surface over the

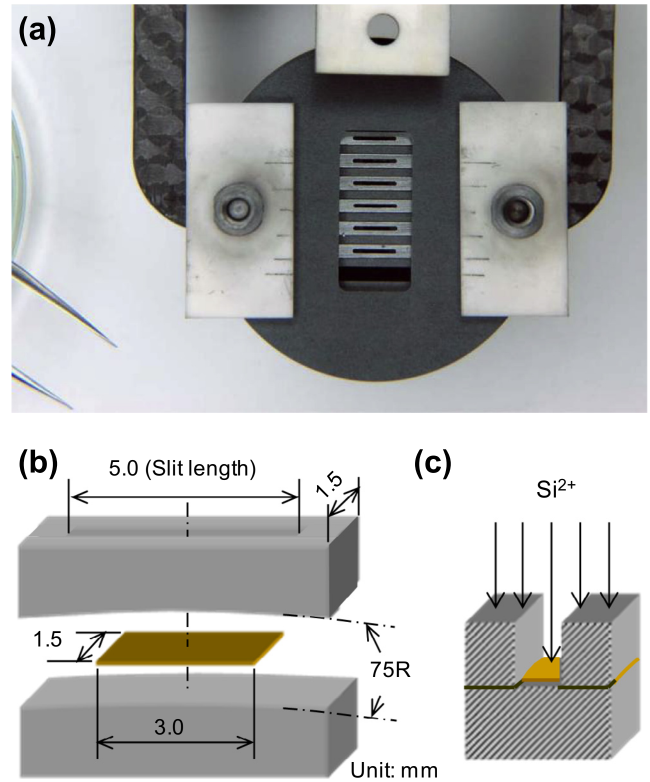

Fig. 1. Specimen holder and samples for the ion irradiation under applied stress. (a) Image of specimen holder after ion irradiation. (b) Schematic of the curved fixtures and sample. (c) Schematic of the fixed sample and ion-beam direction.

entire length of each upper and lower fixture. This radius was selected to apply approximately 25–50% of fracture strength of CVD SiC to the irradiated surface. A 5-mm-long and 0.5-mm-wide rectangular slit was provided at the center of each upper fixture. Specimens were tightly fixed by outer holding fixtures during annealing or irradiation, as shown in Fig. 1 (a). The tensioned surfaces were subjected to ion-beam irradiation, as schematically shown in Fig. 1 (c). Other sets of straight fixtures with similar dimensions and without the curvature were used for the cases of irradiation without stress, and the specimens irradiated without stress are hereafter referred to as control specimens.

2.2. Ion- and post-irradiation experiments

Specimens were preliminarily annealed in the curved fixtures for 1–3 h at the intended irradiation temperature before irradiation to avoid the effects of transient thermal creep during irradiation, which was expected to be significant above 1000 °C [10]. Then, they were irradiated in the Dual-Beam Facility for Energy Science and Technology (DuET) at Kyoto University, which houses 1.7 MV tandem and 1 MV single-end accelerators [11]. The single 5.1 MeV Si^{2+} ion beam was used for inducing displacement damage, which is referred to as a single-ion experiment. An additional He^{+} ion beam with multiple energy (1 MeV and an energy-degraded to 201–737 keV by aluminum foils) was irradiated simultaneously to simulate the (n, α) reaction, which is referred to as a dual-ion experiment. Irradiation temperatures were 280–1200 °C, typically in 100 °C steps. The irradiation fluence of the Si-ions was from 1.2×10^{16} to 3.5×10^{20} ions/m^2, corresponding to 0.001 and 3 dpa (displacement per atom) on average over the damaged range, respectively. The typical flux was 3.5×10^{16} ions/m^2/s corresponding to 3×10^{-4} dpa/s nominally. The depth profiles of displacement damage and concentrations of implanted Si for the 1 dpa average damage level case calculated by SRIM 2003 [12] are shown in Fig. 2. The initial stresses applied at the irradiated surface were 150, 225, and 300 MPa, depending on the specimen thickness.

The specimen curvatures in the stress axis were recorded using an atomic force microscope (AFM) in contact mode with a very compliant cantilever on VN-8000 from KEYENCE. Note that no measurable curvature was detected for all unirradiated specimens randomly selected. The curvature at the centerline parallel to the specimen's long edge was confirmed to be practically uniform for most irradiated specimens over the specimen length, though very limited decrease in the curvature was observed near the edge of highly curved specimens. More than three scatter-free lines of 1 mm length parallel to the long edge near the center were averaged to determine the annealed and/or irradiated curvature.

Thin foils were prepared in a commercial focused-ion-beam unit (JEOL JIB-4500). Microstructures were studied using a transmission electron microscope (TEM, JEOL JEM-2200FS or JEM-2010, 200 keV). Thickness determinations of TEM thin foils were made at several locations by measurement of projected width of the stacking faults.

2.3. Irradiated curvature of the control specimens

Rearrangement of the lattice atoms generally induces mechanical stress in the ion-irradiated regions, primarily through densification or swelling. The accumulation of in-plane compressive stress was expected for SiC on account of the swelling that occurred even in the control specimens irradiated without stress. Some portion of the stress relaxed when specimens were released from the fixtures, but some remained as residual stress. In Fig. 3, the radius of the relaxed curvatures for control specimens of 50 μm thickness are plotted against the logarithm of dpa. It is clear that the specimens immediately became curved after the onset of irradiation; for example, a 3768 mm curvature radius was measured at 1.2×10^{16} ions/m^2 and 800 °C. The rate of decrease in curvature radius was very large, up to $\sim 10^{19}$ ions/m^2, for each irradiation temperature. Then, the reduction rates seemed to saturate above $\sim 10^{20}$ ions/m^2. Note that each value seemed to asymptotically approach a specific value determined by the given

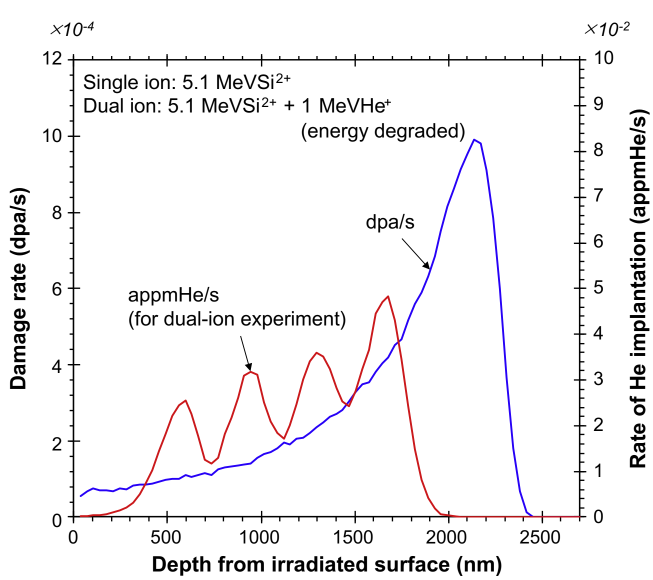

Fig. 2. Depth distribution of rates of displacement damage and concentration of helium calculated by SRIM 2003 [12].

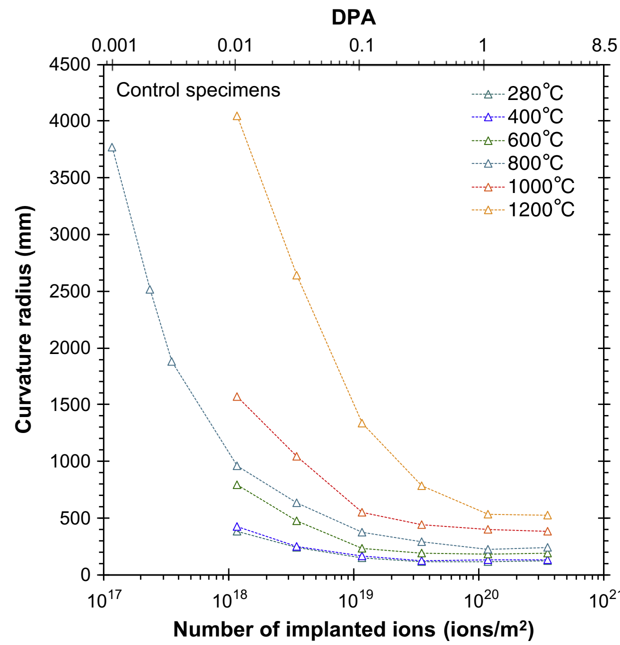

Fig. 3. Curvature radius of the control specimens irradiated at various temperatures without external stress. The radii were measured at RT using the AFM after samples were released from the specimen fixtures.

irradiation temperature. The apparent saturation radius increased with temperature, where radii of 117 and 528 mm were observed at 3.5×10^{16} ions/m^2 (corresponding to 3 dpa) for 280 and 1200 °C, respectively.

Katoh et al. extensively studied ion-irradiation-induced swelling in CVD SiC at DuET [5], the same irradiation facility used in this work. In that work, 3-mm-diameter SiC disks typically 0.25 mm thick were covered with molybdenum mesh during irradiation, and swelling was determined by the step height formed at the boundaries between irradiated and unirradiated surfaces. Because each irradiated area (typically 0.2 mm square) was constrained by the unirradiated regions and ion range was limited to a few microns from the irradiated surface, the measured linear swelling was assumed to be identical with volumetric swelling. The results were well supported by recent neutron irradiation data [2] over a wide temperature range, at least below 3 dpa. In the present work, the constraint in the direction parallel to the specimen's long edge is presumably less significant because of the free end. However, the degree of strain mismatch between the irradiated and unirradiated substrates may be a function of swelling. In Fig. 4, the irradiated curvatures are plotted against the linear swelling estimated at the identical irradiation conditions reported in [5] for each plot, and some missing step-height data was complemented by this work. The irradiated curvatures are practically proportional to the linear swelling for each specimen thickness without any temperature dependence. Therefore, the irradiated curvature of the control specimens can be practically characterized by the linear swelling S_L as follows.

$$\kappa_{irr}^{Control}(\phi) = aS_L(\phi), \tag{1}$$

where $\kappa_{irr}^{Control}(\phi)$ is the irradiated curvature at fluence ϕ and a is the thickness dependent proportional constant. Note that Eq. (1) allows a practical estimation of the surface strain parallel to the specimen's long edge from the irradiated curvature.

The simple equation described above may be understood by considering the in-plane stress induced by local deformation in the irradiated region. Stoney originally solved the relationship be-

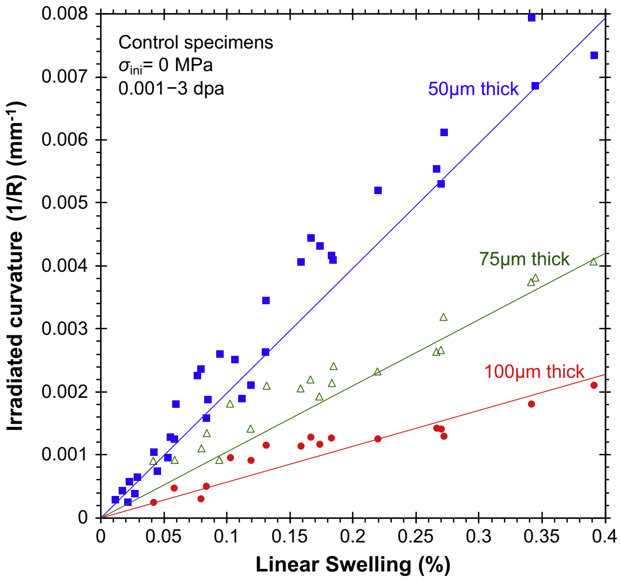

Fig. 4. Relationship between irradiated curvatures of the control specimens and linear swelling measured by step height.

tween the in-plane stress beneath the surface and curvature for analyzing the stress of metallic films deposited electrolytically at the surface of various materials [13]. Flinn et al. further developed this relationship for the integrated stress of irradiated thin specimens as follows [14].

$$\Sigma = \int_0^d \sigma(x)dx = \frac{\kappa E t^2}{6}, \tag{2}$$

where $\sigma(x)$ is the in-plane stress at depth x, κ is the curvature, E is the Young's modulus of the substrate (or unirradiated region), t is the specimen thickness, and d is the damaged depth. Because of the significant damage gradient along the depth as shown in Fig. 2, the local in-plane stress may be different from the average stress given by Σ/d. Because the modulus of SiC is less dependent on the irradiation fluence [2], the average in-plane strain ε_{ave} can be estimated using

$$\Sigma = \int_0^d E_{irr}(x)\varepsilon(x)dx = E_{irr}\varepsilon_{ave}d, \tag{3}$$

where E_{irr} is the irradiated modulus. Then, by assuming that the modulus is unchanged by irradiation, the above equations can be merged as follows:

$$\kappa \propto \varepsilon_{ave}(\Phi)\frac{d}{t^2} \tag{4}$$

where $\varepsilon_{ave}(\phi)$ is the average strain at fluence ϕ. This indicates that the curvature is determined by the strain averaged over the damage range when the irradiation depth and specimen thickness are constant. Because the step height reported in [5], which is integrated out-of-plane strain of the laterally constrained region, is likely proportional to the integrated in-plane strain (or the resultant residual in-plane stress), the results showing linear relation between the irradiated curvature and swelling estimated from step-height measurements would be legitimate. In addition, Katoh's simple manner of determining the nominal dpa, displacements per atom averaged over the damaged range, seems theoretically reasonable to both their and this work according to the above equations. Therefore, the irradiation creep strain was estimated from irradiated curvature by Eq. (1) with some minor corrections arising from variation of sample thickness and irradiated area in this work, and the nominal dpa will be used hereafter.

3. Results

3.1. Swelling–irradiation creep correlation

The curvatures of specimens irradiated with and without stress are compared in Fig. 5, where the corresponding irradiation creep strain and linear swelling are also indicated on secondary axes for reference. The initial external stress at the irradiated surface was 150 MPa for the stressed specimens, though non-negligible reduction in initial stress was expected above 1000 °C because of thermal creep. Thermal creep strain, measured before irradiation, was in agreement with previous thermal creep data for CVD SiC [9,10,15]. The rates of steady thermal creep for CVD SiC were reported to be very small, following the rapid transient creep at moderate stress levels. Therefore, the contribution of thermal creep to the total creep strain cannot be assumed to be a function of irradiation time. This simplification may introduce less than ~1.3% overestimation of irradiation creep strain at 1000 °C assuming 5% more thermal creep strain during irradiation and less than ~6.5% overestimation at 1200 °C assuming 10% more thermal creep strain during irradiation. The error bars indicate the maximum to minimum variation of the measured curvatures. The dotted line indicates the relationship $\kappa_{irr}^{Stressed}/\kappa_{irr}^{Control} = 1$, where κ_{irr}^{m} and $\kappa_{irr}^{Control}$ are curvatures of stressed and control (unstressed) specimens, respectively. Because the irradiated curvature is proportional to the strain at the irradiated surface as shown in Eq. (1), the $\kappa_{irr}^{Stressed}/\kappa_{irr}^{Control}$ ratio simply indicates the ratio of irradiation creep strain and swelling. Although a significant contribution of the thermal creep to the curvature was expected above 1000 °C, irradiation creep strain was defined as the total strain including the contributions of swelling, thermal creep, and irradiation creep.

The plots for specimens irradiated at 280 °C are distributed along the dotted line, indicating the absence of irradiation creep. Most plots above 400 °C are located above the dotted line because of the extra curvature induced by external stress. Note that the linear approximation of the $\kappa_{irr}^{Stressed}/\kappa_{irr}^{Control}$ ratio seems allowable

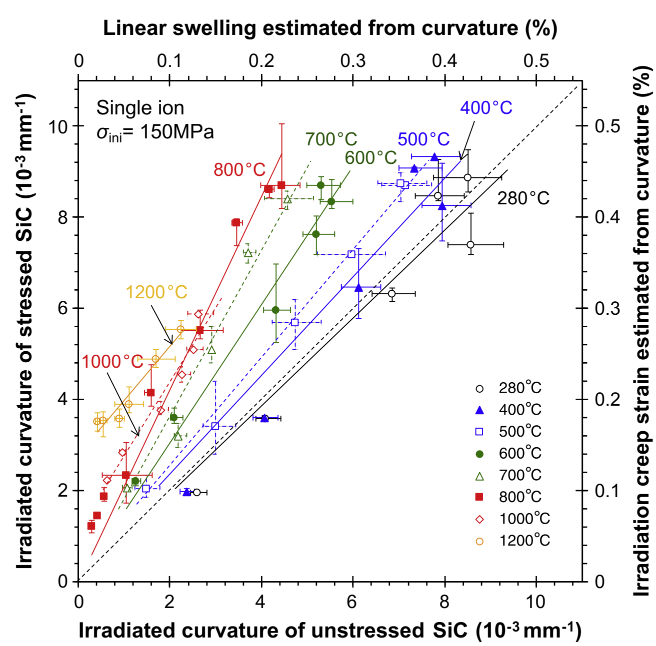

Fig. 5. Relationship between the irradiated curvatures of stressed and unstressed (control) specimens at various irradiation temperatures in single ion experiments.

for the results obtained at respective temperatures. The proportional constant increased with temperature below 800 °C, from ~1.0 at 280 °C to 2.1 at 800 °C. Although the linear relationship appeared to be still maintained at 1000 °C, the constant ratio of 1.6 was significantly smaller than that at 800 °C. The highest irradiation creep rates were found at 800 °C, where the average rates of 2.1×10^{-3}, 2.4×10^{-4}, and 7.8×10^{-6} $dpa^{-1}\,MPa^{-1}$ were estimated in the ranges 0–0.003, 0.01–0.1, and 0.1–1 dpa, respectively. Note that these rates do not include the effect of thermal creep contribution, which was practically finished before irradiation. The saturation of the irradiation creep strain and the linear relationship with swelling are practically consistent with the recent neutron data for CVD SiC [16]. The swelling-creep coupling model, which described their results reasonably well especially at temperatures below 540 °C, was proposed in that work assuming 2D defect clusters are the primary contributor to both the swelling and creep. They estimated the instantaneous creep rates to be $\sim 1 \times 10^{-5}$ $dpa^{-1}\,MPa^{-1}$ at ~0.01 dpa decreasing to $\sim 1 \times 10^{-7}$ $dpa^{-1}\,MPa^{-1}$ at ~1 dpa by the model.

3.2. Stress dependence of irradiation creep strain

External stress was controlled by changing the specimen thickness as already described, where the irradiated surface of thicker specimens was subjected to larger stress. The $\kappa_{irr}^{Stressed}/\kappa_{irr}^{Control}$ ratio, each of which was evaluated from specimens of the same thickness, was plotted against the stress for the irradiation temperatures of 400, 600, and 800 °C. The typical value of the variation in the plots was ±0.2, similar to that of the 150 MPa case. Although it is not clear whether any minor fluence dependence of the $\kappa_{irr}^{Stressed}/\kappa_{irr}^{Control}$ ratio is hidden, the linear relationship of $\kappa_{irr}^{Stressed}/\kappa_{irr}^{Control}$ is still maintained for the 225 and 300 MPa cases. Because swelling is stress independent, the trend of stress dependence in the $\kappa_{irr}^{Stressed}/\kappa_{irr}^{Control}$ ratio is essentially the same as that for irradiation creep strain, though the apparent stress dependence is slightly magnified. Irradiation creep strain showed positive dependence on stress, especially at higher temperatures. In an attempt to approximate the stress effects, the empirical creep equation and corresponding curves or lines are also shown in Fig. 6, assuming the absence of minimum stress for the irradiation

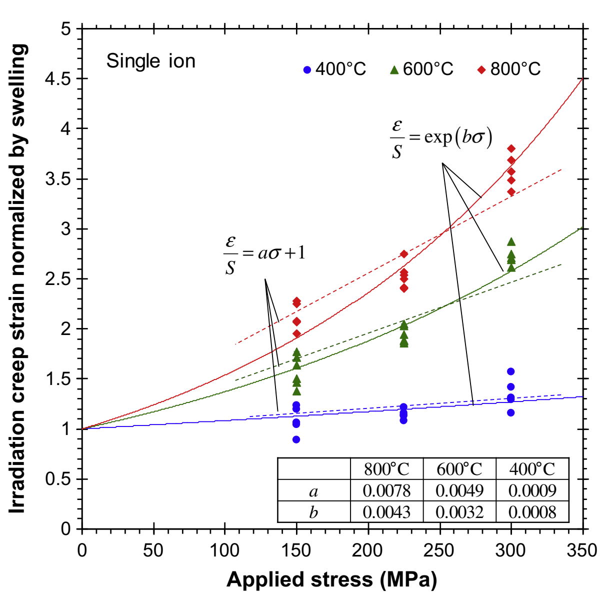

	800°C	600°C	400°C
a	0.0078	0.0049	0.0009
b	0.0043	0.0032	0.0008

Fig. 6. Stress dependence of irradiation creep strain normalized by swelling. Solid and dotted lines are trend lines fitted by approximate equations shown in the figure and inset table.

creep in SiC. The results show that the proportional constant of the linear approximation increased with temperatures from 0.9×10^{-3} at 400 °C to 7.8×10^{-3} at 800 °C. It seems that the exponential approximation also shows a similar temperature dependence. The linear approximation is not applicable at higher stress levels in this work, whereas the exponential approximation shows somewhat better results over a wider stress range at all irradiation temperatures. This implies that the stress exponent n in the historical swelling–creep coupling equation $\dot{\varepsilon} = D\sigma^n\dot{S}$ [17] is more than 1 at higher stress levels, further implying the operation of multiple creep mechanisms. However, further plots will be required, especially at much larger stress levels, for determining the stress effect.

3.3. Irradiation effects on microstructural evolution

Fig. 7 shows the microstructure of SiC irradiated at 800 °C under external stress (300 MPa), the irradiation condition at which the highest creep strain was observed in this work. In each electron beam direction, the corresponding {1 1 1} tetrahedron, in which four surfaces of the tetrahedron correspond to each 1 1 1 family plane, is also shown schematically. All images show the same location in a grain but were taken from slightly different directions using extended diffraction spots, the so-called 1 1 1 reciprocal lattice rod (rel-rod) streaks. Because the 1 1 1 rel-rod generated from planar defects formed on the crystal plane perpendicular to the elongated direction of the streaked spots, the edge-on loops formed on only one crystal plane are shown. That is, all loops in Fig. 7 (a) are formed on $\bar{1}\,\bar{1}\,1$ (denoted as ABD in a {1 1 1} tetrahedron), those in Fig. 7 (b) are formed on $\bar{1}\,1\,\bar{1}$ (denoted as BCD), and those in Fig. 6 (c) are formed on $1\,\bar{1}\,\bar{1}$ (denoted as ADC). Each crystal plane orientation is indicated by the stereo projection viewed from the stress axis of $[0.487\ 5.197\ \overline{1.292}]$ shown in Fig. 7 (d), in which the angles between loop planes and stress axis are described. Although the stress axis is not shown in each image owing to the lack of three-dimensional coordinates on the paper, the beam direction roughly corresponds from the top to bottom of the image.

The results of quantitative analysis of the loop size distribution for each plane are shown in Fig. 8. The normal stress component of each loop plane for loops in Fig. 7 (a–c) was estimated to be 225, 193, and 110 MPa, respectively. The loop number density in the plane with higher normal stress is clearly larger than those in other planes. Although loop size seems to be insensitive to stress, a few larger loops and slightly larger mean sizes were found for the loop plane with higher normal stress, as shown in the figure. The loop plane, which is the aggregates of interstitials, contains extra plane(s) inserted between the original lattice planes. It may require slight lattice dilation in the direction normal to the loop plane, and this is the stress axis indicating the specimen length direction. Therefore, one can say that loops form preferentially on the lattice plane on which a larger normal stress is applied. The contribution of such aligned loops to external stress is discussed later.

3.4. Effect of pre-irradiation on irradiation creep

In the practical case, such that SiC is used for structural or functional materials in nuclear applications, stress will be not only constant but also generated unexpectedly or increase steeply in the middle of reactor operations. In an attempt to simulate these cases, some control specimens irradiated without stress were re-irradiated under applied stress. This may also provide insights into the effects of pre-existing defects on irradiation creep. The results are shown in Fig. 9, where the control specimens pre-irradiated at 400, 600, and 800 °C were re-irradiated to an additional 1 dpa in the curved fixtures at same temperatures as those in the first irradiation. The curvatures after the second irradiation are plotted against

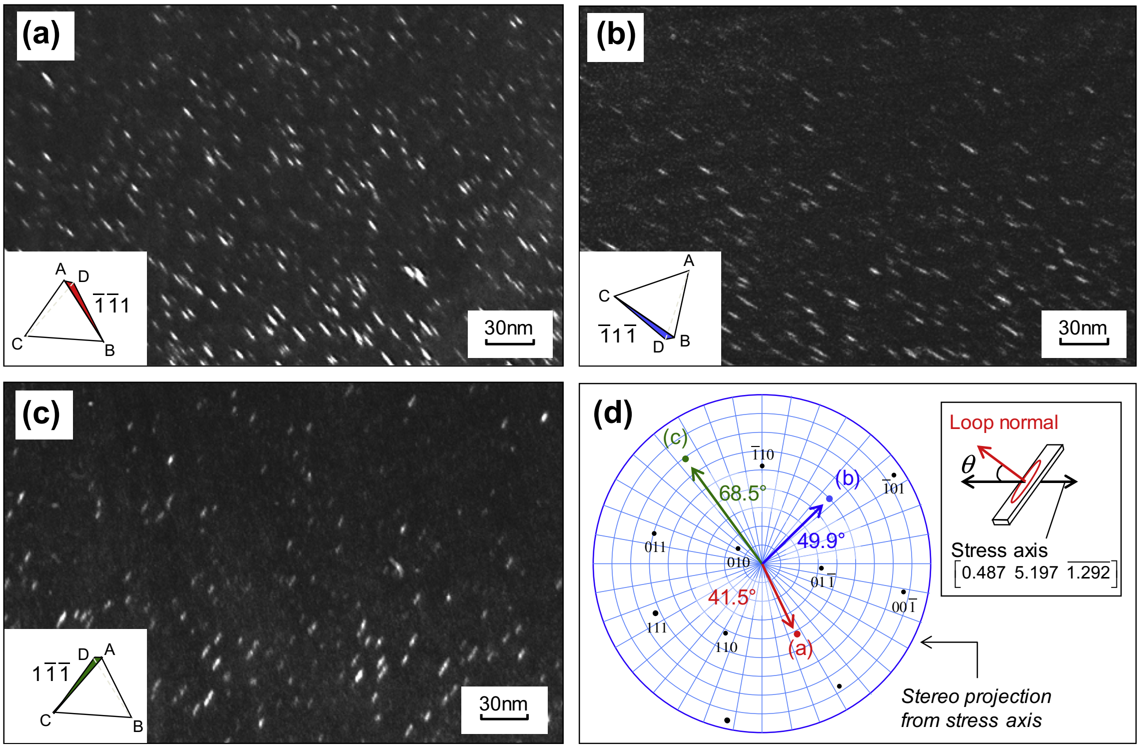

Fig. 7. Microstructure of a sample irradiated with single ions to 3 dpa at 800 °C under σ_{ini} = 300 MPa. Three images show the same location in a grain but were taken from different electron-beam directions, where the edge-on loops formed on (a) $\bar{1}\,\bar{1}\,1$, (b) $\bar{1}\,1\,\bar{1}$, and (c) $1\,\bar{1}\,\bar{1}$ as shown in each image, respectively (see inset Thompson's tetrahedron). Angles between each loop normal and stress axis are indicated by stereo projection in (d).

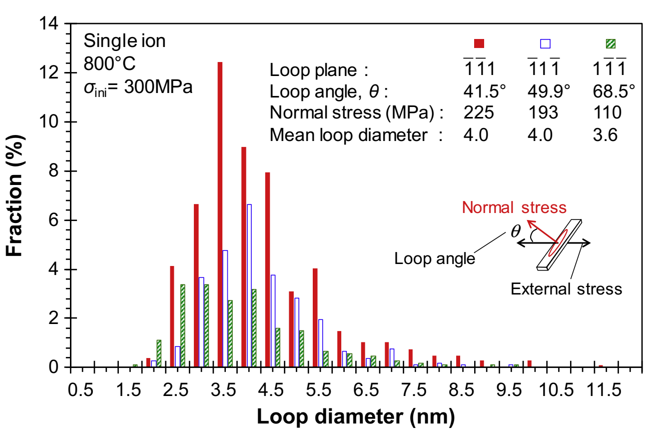

Fig. 8. Size distribution of the Frank loops (see Fig. 7) in a specimen irradiated to 3 dpa at 800 °C under 300 MPa.

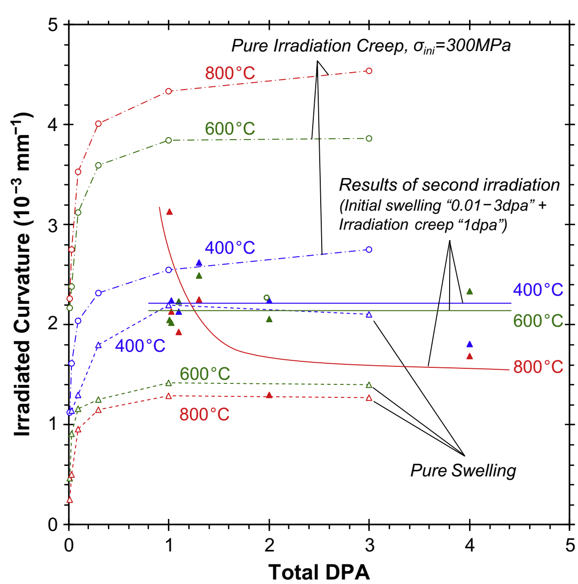

Fig. 9. Effect of pre-irradiation on irradiation creep during second irradiation. The final irradiated curvatures after the second irradiation are plotted against total dpa, and indicated by closed triangular symbols and solid lines. Results measured before the second irradiation (after pre-irradiation without stress) are indicated by open triangular symbols and denoted by pure swelling.

the total damage level. In addition, the irradiated curvature of the control specimens is also plotted in the figure for reference; note that these curvatures are the swelling-induced and initial curvatures before the second irradiation. Other reference plots denoted as pure irradiation creep in the figure are the results for specimens irradiated under applied stress (300 MPa) from the beginning. It is clear that most curvatures after the second irradiation never reached the referential curvature denoted as pure irradiation creep at a comparable damage level, though minor extra curvatures were observed for most specimens after the second irradiation. The curvatures of the specimens re-irradiated at 400 and 600 °C were rather constant and seemed to be independent of the total damage level. Almost no and only ~58% of the referential curvature was measured at 400 °C and 600 °C after the second irradiation, respectively. At 800 °C, the re-irradiated curvature seemed to depend on the damage level, where approximately 70% and 40% of the pure irradiation creep strain was observed at 1.01 total dpa and 2 total dpa, respectively. The significant reduction in the initial stress before the second irradiation is probably not the reason for the limited creep strain, as the results of the second irradiation do not depend on fluence, especially at lower temperatures (for which a significant fluence dependence of swelling was observed). Therefore, irradiation creep at the second irradiation can be concluded to be retarded by the very short first irradiation without stress.

3.5. Transmuted He effects on irradiation creep

In a manner similar to the single-ion cases, both the curved and straight (control) specimens of 50 μm thickness (with an initial stress of 150 MPa for curved specimens) were irradiated with dual ions at 400, 600, and 800 °C. In Fig. 10, the irradiated curvatures of the stressed specimens are plotted against those of the comparable unstressed specimens. The average rate of helium deposition was 60 appm He/dpa in the dual-ion-irradiated range, i.e., from 0.5 to 1.8 μm as shown in Fig. 2. The simultaneous helium implantation to SiC has been reported to enhance swelling at 400–800 °C [5]. The swelling estimated from the irradiated curvatures of the control specimens irradiated with dual ions was consistent with that in the previous report. This may permit a comparison between irradiation creep strain and swelling in a manner similar to the single-ion case, despite the somewhat localized distribution of helium. In contrast to the significant enhancement of swelling by helium, however, the helium effect on irradiation creep seemed to be very limited at all irradiation temperatures except for very low fluence. For example, the linear swelling/irradiation creep at 0.01 dpa (0.6 appm He) was estimated to be 0.09/0.16% at 400 °C and 0.05/0.1% at 800 °C. In addition, the linear swelling/irradiation creep at 3 dpa (180 appm He) was estimated to be 0.48/0.48% at 400 °C and 0.23/0.25% at 800 °C. Note that the estimated $\kappa_{irr}^{Stressed}/\kappa_{irr}^{Control}$ ratio is similar or slightly higher than that of single-ion cases below 0.03 dpa (1.8 appm He) at all temperatures. This indicates that the observed helium effect depends strongly on the concentration of helium or He/dpa ratio.

Fig. 11 (a and b) shows the microstructure of the specimen irradiated with dual ions to 3 dpa at 800 °C under an applied stress of 150 MPa. Similar to Fig. 6, both images show identical locations in a grain, but those were taken from a different foil tilt. Because the foil surface of this selected grain roughly corresponds to the ⟨1 0 0⟩ direction, the approximate stress axis can be written as indicated by arrows in each image. Under the conditions studied here, Frank

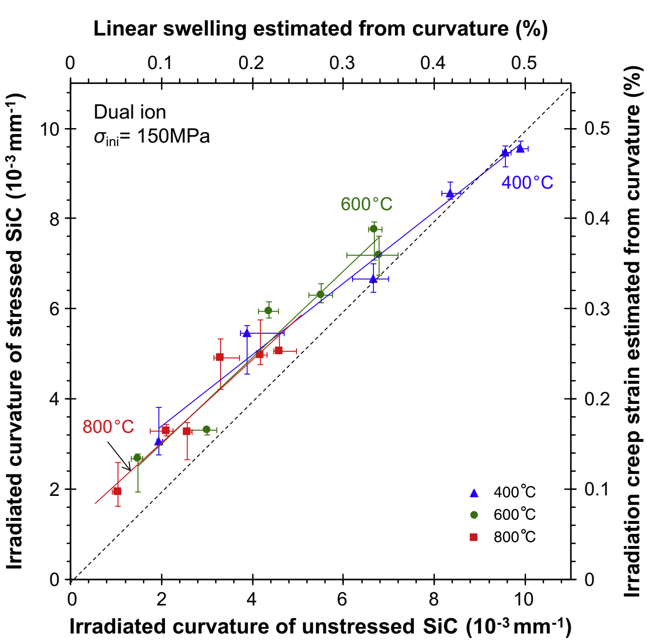

Fig. 10. Relationship between the irradiated curvatures of stressed and unstressed (control) specimens in dual ion experiments.

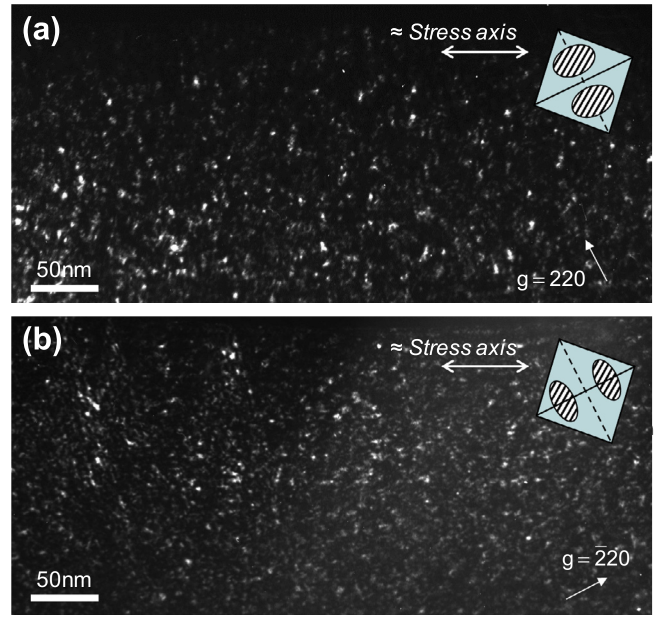

Fig. 11. Microstructure of a sample irradiated with dual ions to 3 dpa at 800 °C under σ_{ini} = 150 MPa. Both images of (a and b) show the identical location in a grain but were taken from different electron-beam directions. Loop planes of visible Frank loops are schematically indicated by the shaded area in the Thompson's tetrahedron insert in each image.

loops appeared on two of four {1 1 1} planes in each image using either the (a) g = 200 or (b) g = 020 diffraction condition as schematically shown, and others had disappeared because of the $g{\cdot}b$ = 0 condition. The normal stress for loops in Fig. 11 (a) is clearly smaller than that in Fig. 11 (b) because of the very large angle between the stress axis and loop normal, approximately 64° for both the two loop planes with respect to external stress. Most loops were observed as black dots or very small loops, and in this case, neither 1 1 1 rel-rods nor streaks were detected in the diffraction spots probably because of their small size in contrast to the single-ion case. The mean loop diameter was 2.6 nm for non-aligned loops and 2.8 nm for relatively aligned loops, both of which are significantly smaller than those of the loops found in the single-ion-irradiated specimen (see Fig. 8). The size distributions of each loop are shown in Fig. 12. The total number density of the loops is 2.4×10^{23} m^{-3}, which is more than twice than that of the loops in the specimen irradiated with single ions at the same fluence and temperature under higher applied stress (300 MPa). Although the size peak for non-aligned loops seems to be somewhat sharp compared to that for aligned loops, no significant difference in the size distribution between favorable and unfavorable loops was detected for the dual-ion case.

3.6. Recovery of the dimensional change

Specimens irradiated to 1 dpa at 400 and 800 °C were annealed in a vacuum furnace for typically 30 min at 200–1500 °C in increments of 100 °C to study the recovery of the swelling and irradiation creep strain. The annealed curvature was measured at room temperature after being annealed at each temperature. Note that the specimens were not fixed on any fixture during annealing; therefore, some compression stress was expected in the irradiated region. The annealed curvatures normalized by the as-irradiated curvature for specimens irradiated at 400 and 800 °C are shown in Fig. 13 (a and b), respectively, and each figure includes plots for both single- and dual-ion cases for comparison. In Fig. 13 (a), recovery began at the irradiated temperature of 400 °C, and more

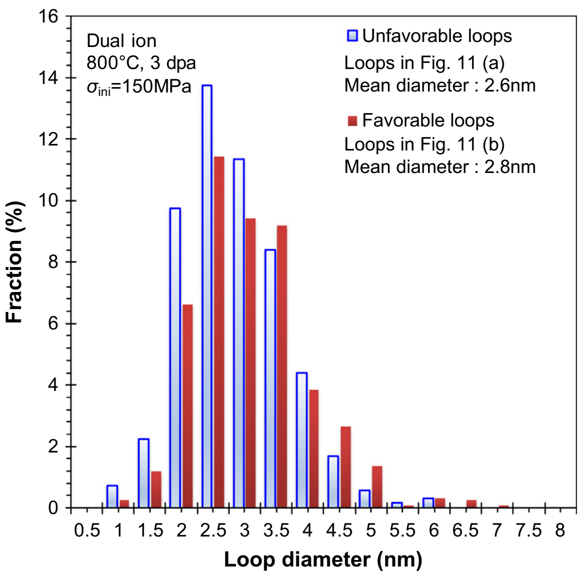

Fig. 12. Size distribution of the Frank loops formed on aligned and non-aligned planes with respect to the external stress in specimens irradiated with dual ions to 3 dpa at 800 °C under σ_{ini} = 150 MPa.

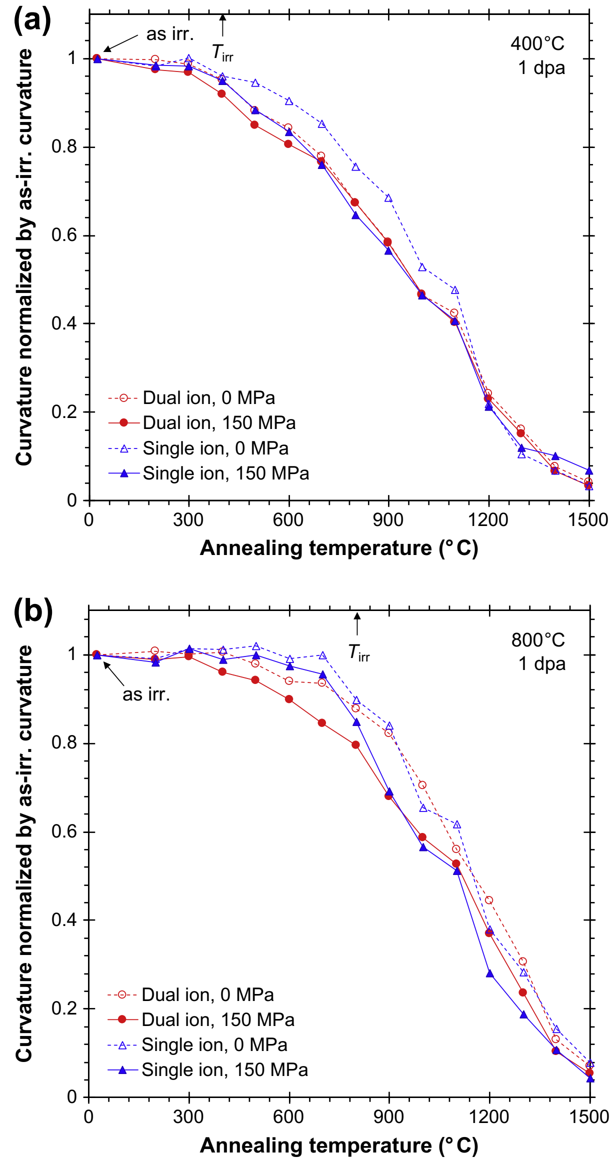

Fig. 13. Recovery behavior of the irradiated curvatures.

than 95% of the as-irradiated strain was recovered at 1500 °C for all specimens. Although the recovery rate of swelling in single-ion-irradiated specimens (open triangle) seems to be smaller than those in other specimens below 1000 °C, a similar recovery trend was observed for all other specimens. In Fig. 13 (b), recovery of the single-ion cases began at the irradiation temperature of 800 °C. Then, somewhat steep recovery is observed above this temperature. On the other hand, the recovery of dual-ion-irradiated specimens, especially stressed specimens, is found at temperatures significantly lower than the irradiation temperature. This is unexpected because the damage level of 1 dpa seems to be enough to reach a mature microstructure at 800 °C. No significant differences were observed for the final curvatures of each specimen after annealing at 1500 °C, which is a similar value to that observed for specimens irradiated at 400 °C. These recovery behaviors may be attributed to the recovery of microstructural defects, where the slight remaining strain observed after annealing at 1500 °C is probably responsible for the vacancy-related clusters, similar to those reported by positron annihilation spectroscopy [18]. Further discussion is contained in the following section.

4. Discussion

In this work, the irradiation creep of SiC, which was found above 400 °C for the single-ion case, was studied by an ion-irradiation method. First, it should be pointed out that a temperature-dependent linear relationship between irradiation creep strain and swelling was observed at 400–800 °C, as shown in Fig. 5, indicating dpa dependence of irradiation creep strain similar to that of swelling. This has recently been reported for neutron-irradiated SiC, and a linear coupling equation between swelling and irradiation creep strain was proposed in [16] as described above. The general trend of the SiC swelling was reported to be roughly proportional to the logarithm of dpa at <0.03–0.05 dpa depending on temperature, with the swelling rates gradually decreasing with damage accumulation [5]. Swelling reaches the saturation value defined by the irradiation temperature, except for the temperature at which void swelling commences (above 1000 °C) or amorphization is dominant (below ∼150 °C depending on the species of incident particle or energy), and then the saturation value begins to continuously decrease with increasing temperature at $\sim$150 < T_{irr} < 1000 °C. These trends may be understood from knowledge of the microstructural development. Swelling is believed to be due to the accumulation of point defects such as vacancies, interstitials, antisites, and tiny defect clusters in the temperature range. Because self-interstitial atoms (SIAs), perhaps C interstitials, are believed to be mobile by about 200 °C [19,20], most SIAs produced by displacement are expected to recombine with vacancies or form SIA clusters with each other in the early irradiation regime [21,22] at >∼200 °C. The population of these defects increases rapidly with fluence in the transient swelling regime. Therefore, most point defects may be mutually annihilated or captured immediately by dense SIA clusters (after they are produced) if the mobility of the vacancies is not significant. These may be responsible for the rapid increase in swelling below ∼0.05 dpa, and the saturated swelling is essentially determined by the equilibrium population of defects at a given irradiation temperature. Although the fraction of the swelling contribution within the defects listed above is not clear, the relative contribution of point defects such as single vacancies probably decreases with increasing temperature because of the significant reduction in the defect density. In turn, the relative contribution of tiny SIA clusters may increase at higher temperatures. Because the net diffusivity of the SIAs was reported to still be limited below 1000 °C due to the significant sink density, the growth rates of SIA clusters are still limited at 800 °C [23,24]. Indeed, the formation of Frank loops or small loops, which can be distinguished from so-called black dots, was reported in SiC irradiated above ~600 °C for neutron work [3,25] and above 800 °C for ion-beam work [26]. Therefore, the contribution of SIA clusters with even higher number densities to swelling is probably significant and dominant at 400–800 °C.

On the other hand, irradiation-induced creep or anisotropic strain in cubic SiC essentially requires stress-assisted defect motion in addition to the number of contributors. The limited thermal mobility of most defects at 280 °C is probably responsible for the absence of irradiation creep. Although carbon interstitials are mobile and form tiny, dense SIA clusters with each other at 280 °C as stated above, most SIA clusters found in SiC irradiated with neutrons at 300 °C have been reported to be less than 1 nm in apparent diameter [26]. Because the size corresponds to the resolution limit of the conventional TEM used in that work, TEM-invisible SIA clusters presumably are the dominating defects at 280–300 °C. SIA clusters survived the intracascade recombination, with each cluster typically containing several to 100 atoms and being shaped like small prismatic dislocation loops with radial dimensions of 1–3 nm for the metals [27], is also a possible condensation center for SIAs. The orientation may be affected by external stress during nucleation and may cause the anisotropic loop distribution. For SiC, however, only a few and very small SIA clusters, each containing less than three or four atoms, have been theoretically found [28,29]. Because these tiny SIA clusters seem to be too small to induce anisotropic lattice dilation because of their poor two-dimensional shape, defect size, in addition to defect mobility, is probably insufficient to induce the irradiation creep at low temperatures despite the significant defect population.

Above 400 °C, at which irradiation creep becomes measurable, the tiny, dense microstructural features are still maintained; however, the diameter of SIA clusters formed at 400 °C was from 1 to 3 nm [26], indicating a significant increase in the SIAs' net mobility compared to that at 280 °C. Therefore, the irradiation creep observed above 400 °C can probably be attributed to stress-assisted motion in the thermally mobile defects. The most notable stress effect on the microstructural development is the anisotropy of the Frank loop distribution, which was found at 800 °C as shown in Figs. 7 and 8. This characteristic loop distribution is commonly known as the stress-induced preferential nucleation of loops (SIPN) [30–32] or stress-induced preferential absorption (SIPA) [33,34] for pure metals and alloys, where nucleation or growth of interstitial loops depends on their orientation with respect to the external stress axis. These are typically interrelated with a number of other irradiation creep mechanisms in metals [35], such as the climb-induced glide mechanisms [17], which cause dislocations of different orientations to climb at different rates. When the glide processes of the dislocations are neglected, as in the case of SiC, the lattice dilation caused by the anisotropic distribution of the loops and 2D SIA clusters directly contributes to the anisotropy of the macroscopic strain.

Anisotropic loop formation in SiC has been reported in specimens irradiated with an ion beam at 1400 °C [36]. The fraction of loops formed on the 111 plane nearly parallel to the irradiated surface was significantly larger than that on the other 111 planes in a grain. The strain constraint, except in the direction toward the free surface end, was concluded to be responsible for the lower loop density for the other 1 1 1 planes. Slight but measurable anisotropy of the loop distribution was also reported in neutron work for SiC irradiated under applied bend stress at 1000 °C [26]. Both results, however, showed that stress has an insignificant effect on defect size, which is consistent with the present result. These results indicate that the SIPA operation is somewhat limited in SiC even at high temperatures. The absence of, or very limited, strain after the second irradiation following the first irradiation without stress supports the insignificant contribution of the SIPA mechanism to irradiation creep (see Fig. 9). The exception of the re-irradiation results for the specimen initially irradiated to 0.01 dpa at 800 °C, in which significant strain was induced by the second irradiation, was presumably due to the very low number density of the defects and unfinished nucleation of SIA clusters at the damage level of the first irradiation.

Strain in both the stressed and control specimens of 50 μm thickness irradiated to 0.01 or 0.1 dpa is shown in Fig. 14 as a function of irradiation temperature. Irradiation creep strain (solid lines) seems to be independent of irradiation temperature from 400 to 800 °C because the temperature dependence of creep strain is contrary to the negative temperature dependence of linear swelling at this temperature range. Assuming that both stressed and control specimens have SIA clusters of similar density and the primary contributor to strain is SIA loops at 400–800 °C, the differential strain between the stressed and control specimens (the difference between the solid and dotted lines in Fig. 14) is primarily attributable to the magnitude of the loop anisotropy. The temperature-dependent discrepancy between the two, as shown in Fig. 14, indicates that the fraction of the aligned defects and loop area increases with irradiation temperature at 400–800 °C. This also implies that more than 35% and 50% of SIA clusters including Frank loops were aligned to the external stress at 600 and 800 °C, respectively. The discontinuous drop observed for the 1 dpa case at 1000 °C is probably caused by the rapid decrease in loop density, as observed in unstressed SiC [26]. Although further analysis may be required to determine the primary irradiation creep mechanism in SiC, the anisotropic distribution of SIA clusters taking planar shape is the most probable. This is probably caused by SIPN and/or the rotation of initial interstitial clusters very early in the irradiation regime. Note that a linear relationship between irradiation creep strain and swelling was observed at all stress levels, indicating that the fraction of loops aligned in respect to the external stress is dependent on stress level, in addition to temperature.

The effects of helium on swelling has also been reported for SiC irradiated with dual ions at a wide temperature range [5], where

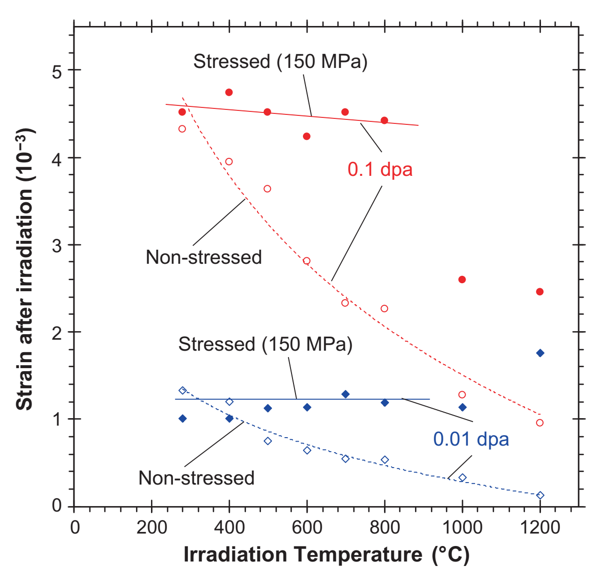

Fig. 14. Comparison of a temperature-dependent strain between stressed and non-stressed specimens irradiated with single ions.

much larger swelling at 400–800 °C was found in dual-ion-irradiated specimens than that in single-ion-irradiated specimens. Because helium has an extremely low solubility in most irradiated materials, it generally has a strong tendency to precipitate into helium bubbles, which are vacancy clusters filled with helium gas. It has been speculated that the increasing number of vacancies stabilized by helium atoms is the underlying mechanism for the enhanced swelling [5], although the helium bubbles have been generally observed in SiC above 10 dpa at >1000 °C under He/dpa ratio conditions similar to those in this work [37,38]. Although the effects of helium on irradiation creep in SiC are also expected to be significant because of the strong interdependence between creep and swelling as demonstrated, no report is currently available. In contrast to the results on enhanced swelling, however, Fig. 10 clearly shows that helium suppressed irradiation creep, especially at the conditions inducing much swelling. This probably can be attributed to the lack of significant anisotropy in the loop distribution, as shown in Figs. 11 and 12. It is also important to note that the recovery of the specimen irradiated with dual ions was observed significantly below the irradiation temperature, as shown in Fig. 13 (b). Thermal helium desorption of 3C–SiC irradiated with helium ions below 100 °C has been reported to occur at 800–900 °C or above 1000 °C depending on the implantation energy [39,40]. The low temperature peak was found only in specimens irradiated with very low energy He ions, which was attributed to interstitial helium or helium trapped by the near-surface sites. High temperature peaks were generally observed for specimens irradiated with MeV He ions, which is a condition somewhat comparable to this work. Such peaks are thought to be related to the detrapping of helium from He-vacancy clusters. Therefore, the recovery found below 800 °C may not be related to helium desorption but, rather, implies that the defects formed in the specimen were more unstable than others at the irradiation temperature, probably because of their small size. If the loop orientation was determined at very low fluence as discussed above, helium and/or the dense vacancies stabilized by helium atoms would affect the orientation of the nuclei of SIA clusters.

5. Conclusion

The irradiation creep of high-purity 3C–SiC produced by CVD was studied by an ion-irradiation method under various conditions. Thin specimens were fixed in curved fixtures equipped with a slit and tensioned surface and then subjected to ion irradiation through the slit. The surface strain was successfully estimated from the irradiated curvature on the basis of results that showed a linear dependence between the curvature and swelling estimated from the step height of specimens irradiated without stress. Comparing the irradiated curvatures of stressed and non-stressed specimens provided the following information: (1) irradiation creep was absent at 280 °C, (2) irradiation creep strain and swelling exhibited a linear relationship at 400–800 °C, (3) the proportional constant increased with temperature and stress, and (4) irradiation creep strain was somewhat limited above 1000 °C. Microstructural analysis revealed significant anisotropic distribution of Frank loops in a stressed specimen irradiated at 800 °C, which was suspected to be the primary irradiation creep mechanism of SiC. The very limited defect mobility, therefore, is probably responsible for the lack of creep strain at 280 °C. The results of re-irradiation under stress after irradiation without stress, in which irradiation creep was significantly retarded by the pre-irradiation to 0.01 dpa at 400 and 600 °C, imply that the orientation of the loops including SIA clusters was determined very early in the irradiation, at least below 0.01 dpa. The insignificant stress dependence on the defect size also supports this conclusion. For dual-ion cases, irradiation creep was absent or very limited at all irradiation temperatures studied (400–800 °C). Microstructural analysis and strain recovery behavior indicated that helium inhibited the stable growth of SIA clusters and prevented them from exhibiting anisotropic distribution.

Acknowledgements

This work was supported by JSPS KAKENHI Grant Number 24760715.

References

[1] R.J. Price, Nucl. Technol. 35 (1977) 320–336.
[2] L.L. Snead, T. Nozawa, Y. Katoh, T.S. Byun, S. Kondo, D.A. Petti, J. Nucl. Mater. 371 (2007) 329–377.
[3] R.J. Price, J. Nucl. Mater. 48 (1973) 47.
[4] H. Inui, H. Mori, A. Suzuki, H. Fujita, Philos. Mag. B 65 (1992) 1–14.
[5] Y. Katoh, H. Kishimoto, A. Kohyama, J. Nucl. Mater. 307–311 (2002) 1221–1226.
[6] Y. Katoh, L.L. Snead, I. Szlufarska, W.J. Weber, Curr. Opin. Solid State Mater. Sci. 16 (2012) 143–152.
[7] R.J. Price, in: HTGR Base Program Quarterly Progress Report for the Period Ending August 31, General Atomic Division of General Dynamics, Report GA-8200, 1967, p. 91.
[8] R. Scholz, J. Nucl. Mater. 258–263 (1998) 1533–1539.
[9] Y. Katoh, L.L. Snead, Ceram. Eng. Sci. Proc. 26 (2005) 265–272.
[10] K. Shimoda, S. Kondo, T. Hinoki, A. Kohyama, J. Eur. Ceram. Soc. 30 (2010) 2643–2652.
[11] A. Kohyama, Y. Katoh, M. Ando, K. Jimbo, Fusion Eng. Des. 51–52 (2000) 789–795.
[12] J.F. Ziegler, Nucl. Instrum. Methods B 219–220 (2004) 1027–1036.
[13] G.G. Stoney, Proc. R. Soc. London Ser. A 82 (1909) 1729.
[14] P.A. Flinn, D.S. Gardner, W.D. Nix, IEEE Trans. Electron. Dev.; W. Corbett, J.P. Karins, T.Y. Tan, Nucl. Instum. Methods ED-34 (1987) 689.
[15] K. Abe, S. Nogami, A. Hasegawa, T. Nozawa, T. Hinoki, J. Nucl. Mater. 417 (2011) 356–358.
[16] Y. Katoh, L.L. Snead, C.M. Parish, T. Hinoki, J. Nucl. Mater. 434 (2013) 141–151.
[17] J.H. Gittus, Phil. Mag. 25 (1972) 345.
[18] H. Itoh, A. Uedono, T. Ohshima, Y. Aoki, M. Yoshikawa, I. Nashiyama, S. Tanigawa, H. Okumura, S. Yoshida, Appl. Phys. A 65 (1997) 315–323.
[19] H. Itoh, N. Hayakawa, I. Nashiyama, E. Sakuma, J. Appl. Phys. 66 (1989) 4529.
[20] H. Itoh, A. Kawasuso, T. Ohshima, M. Yoshikawa, I. Nashiyama, S. Tanigawa, S. Misawa, H. Okumura, S. Yoshida, Phys. Status Solidi A 162 (1997) 173–198.
[21] M. Bockstedte, A. Mattausch, O. Pankratov, Phys. Rev. B 69 (2004) 235202.
[22] A. Mattausch, M. Bockstedte, O. Pankratov, Phys. Rev. B 69 (2004) 045322.
[23] S. Kondo, Y. Katoh, L.L. Snead, J. Nucl. Mater. 382 (2008) 160–169.
[24] S. Kondo, Y. Katoh, L.L. Snead, Phys. Rev. B 83 (2011) 075202.
[25] T. Yano, H. Miyazaki, M. Akiyoshi, T. Iseki, J. Nucl. Mater. 253 (1998) 78.
[26] Y. Katoh, N. Hashimoto, S. Kondo, L.L. Snead, A. Kohyama, J. Nucl. Mater. 351 (2006) 228–240.
[27] D.J. Bacon, A.F. Calder, F. Gao, V.G. Kapinose, S.J. Wooding, Nucl. Instrum. Methods B 102 (1995) 37.
[28] F. Gao, W.J. Weber, Phys. Rev. B 63 (2000) 054101.
[29] R. Devanathan, W.J. Weber, F. Gao, J. Appl. Phys. 90 (2001) 2303.
[30] A.D. Brailsford, R. Bullough, Phil. Mag. 27 (1973) 49.
[31] R.V. Hesketh, Phil. Mag. 7 (1962) 1417.
[32] G.W. Lewthwaite, J. Nucl. Mater. 46 (1973) 324.
[33] P.T. Heald, M.V. Speight, Phil. Mag. 29 (1974) 1075–1080.
[34] W.G. Wolfer, M. Ashkin, J. Appl. Phys. 46 (1975) 547–557.
[35] R. Bullough, M.H. Wood, J. Nucl. Mater. 90 (1980) 1.
[36] S. Kondo, A. Kohyama, T. Hinoki, J. Nucl. Mater. 367–370 (2007) 764–768.
[37] S. Kondo, K.H. Park, Y. Katoh, A. Kohyama, Fusion Sci. Technol. 44 (2003) 181.
[38] A. Hasegawa, S. Nogami, S. Miwa, K. Abe, T. Taguchi, N. Igawa, Fusion Sci. Technol. 44 (2003) 175.
[39] E. Oliviero, M.F. Beaufort, J.F. Barbot, A. van Veen, A.V. Fedorov, J. Appl. Phys. 93 (2003) 231.
[40] A. Hasegawa, B.M. Oliver, S. Nogami, K. Abe, R.H. Jones, J. Nucl. Mater. 283–287 (2000) 811–815.